Quantum measurement of a double quantum dot coupled to two kinds of environment

Lisha Kang, Yanhui Zhang,* Xiulan Xu, and Xu Tang
College of Physics and Electronics, Shandong Normal University, Jinan 250014, China
(Received 5 August 2017; revised manuscript received 11 November 2017; published 12 December 2017)

We theoretically study the quantum measurement of a double quantum dot coupled to environments by Bloch equations with an additional vector. Using a quantum point contact as a detector, we accurately calculate the current, the Fano factor, and the waiting time, respectively, to characterize the dynamical properties in two kinds of environments. In the dissipative case, the asymmetrical Fano factor is enhanced with the increase in deocoherence rates and suppressed as the growth of relaxation rates, and the super-Poissonian noise is mainly due to the effects of a dynamical channel blockade and quantum coherence. In the pure dephasing case, the symmetrical Fano factor is magnified, which can be attributed to the quantum Zeno effect. Moreover, we show that the distribution of the average waiting time exhibits good agreement with the variation tendency of the current. Our paper provides an effective method in handling quantum measurement.

DOI: 10.1103/PhysRevB.96.235417

I. INTRODUCTION

Quantum measurement has drawn much extensive attention in the mesoscopic field, which has further applications in understanding quantum entanglement, quantum coherence, quantum phase transition, and quantum control [1–10]. Generally, in the field of quantum information processing and quantum computing, the environments play an important role in an open quantum system [11–13]. It mainly is related to the inherent mechanism of decoherence and relaxation dynamics which have not been studied thoroughly so far. Moreover, the dynamical properties influenced by the decoherence and relaxation processes are still a hot research topic.

The double quantum dot (DQD) provides a useful model to explore the relation between the environments and the effects of decoherence and relaxation dynamics in quantum measurement [14–19]. The quantum point contact (QPC) obviously is regarded as a sensitive charge detector. In fact, more interesting quantum effects can be studied by the measuring qubit when the interaction strength between the system and the environment is known. Recently, shot noise and average waiting time have already been regarded as the indicators of the fluctuations induced by the interaction between the system and its environments in mesoscopic transport [20–25]. In the past few years, many prominent methods have been proposed to study the quantum transport and quantum measurement [12,26–29]. As a matter of fact these methods are equivalent despite exhibiting different forms.

Many properties of the DQD can be studied within the framework of full counting statistics both in theory and in experiments [30–38]. The statistical cumulants of the number of the transferred electrons present different kinds of physical features [16,30,31,37]. Two important physical quantities are the average current and the Fano factor, which are the first and second cumulants. Here, the Fano factor $F = 1$, $F > 1$, or $F < 1$ represents the Poissonian, super-Poissonian, and sub-Poissonian noise, respectively. The effects of dephasing and dissipation processes in conductors were studied on the suppression of current shot noise within the framework of scattering theory [39]. Moreover, the quantum Zeno effect can be expected to analyze noise properties in the measurement, which has been studied excellently from theoretical to experimental investigations in recent years [40–43].

In this paper, we use the Bloch equations with an additional Bloch vector to study the quantum measurement of a DQD in the dissipative and pure dephasing environments based on full counting statistics. In particular, we accurately calculate the detector current, the Fano factor, and the waiting time to express the dynamical properties. In the dissipative environment, we unambiguously demonstrate that the effects of the dynamical channel blockade and quantum coherence cause the enhancement of the Fano factor. A close relationship between the super- or sub-Poissonian noise and different inherent mechanisms is revealed. It is illustrated further that the Fano factor can be suppressed strongly due to different relaxation rates and enhanced according to different decoherence rates. In the pure dephasing environment, the results show the symmetry of the current and the Fano factor. Moreover, the most interesting result is that the quantum Zeno effect has been found in the analysis. In addition, there is good agreement between the distribution of the average waiting time and the variation tendency of the current. Our results and analysis cannot only reveal the inherent dynamical mechanism of electron transfer in the DQD, but also promote the development of the theoretical framework of quantum measurement.

The paper is organized as follows. In Sec. II we describe the measurement of a DQD by a QPC in the framework of the density matrix. The Bloch equations with an additional vector also are described. Correspondingly, the detailed equations for the cumulants of electron countings are presented. In Secs. III and IV, we use our method to investigate the dynamical properties of the current, the associated Fano factor, and the waiting time, respectively, through the DQD. Results based on the dissipative and pure dephasing environments are discussed. In addition, the dynamical channel blockade effect and quantum Zeno effect are explored in our paper. Moreover, a brief conclusion is presented in Sec. V.

II. THEORETICAL FRAMEWORK

We consider a two-level qubit system measured by a QPC as schematically shown in Fig. 1. The Hamiltonian of the whole

*yhzhang@sdnu.edu.cn

 ©2017 American Physical Society

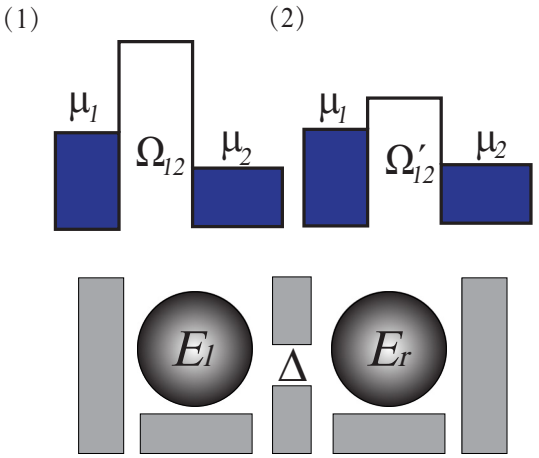

FIG. 1. Schematic for the DQD monitored by a QPC detector. The position of the electron in the left or right dot generates two different states of the detector (1) and (2). $\mu_{1,2}$'s denote the chemical potential in the left and right reservoirs.

system is written as

$$H = H_S + H_{\rm PC} + H_I, \tag{1}$$

where

$$\begin{aligned} H_S &= -\frac{\varepsilon}{2}(a_l^\dagger a_l - a_r^\dagger a_r) - \Delta(a_l^\dagger a_r + a_r^\dagger a_l), \\ H_{\rm PC} &= \sum_{i=1,2} E_i a_i^\dagger a_i + \sum_{1,2}(\Omega_{12} a_2^\dagger a_1 + \Omega_{12}^* a_2 a_1^\dagger), \\ H_I &= \sum_{1,2} \delta\Omega_{12} a_r^\dagger a_r (a_2^\dagger a_1 + a_1^\dagger a_2) \end{aligned} \tag{2}$$

are the Hamiltonians of the DQD, the QPC, and the interaction Hamiltonian, respectively [26]. Here, $a_{l,r}^\dagger(a_{l,r})$ is the electron creation (annihilation) operator for the electron in the DQD, and $a_{1,2}^\dagger(a_{1,2})$ is the same operator of the left and right reservoirs in the QPC; $E_{l,r} = \mp\varepsilon/2$, and Δ is the coupling between the states $E_{l,r}$ [44]; Ω_{12} is the hopping amplitude between the states E_1 and E_2 of the QPC; the interaction term H_I gives rise to a change in the hopping amplitude $\delta\Omega_{12} = \Omega_{12} - \Omega_{12}^{'}$, depending on which dot is occupied [27].

The dynamical evolution of the reduced system, which is described by the reduced density-matrix $\rho(t)$, is obtained by the Liouville equation,

$$\frac{\partial}{\partial t}\rho(t) = -\frac{i}{\hbar}[H,\rho(t)] + \mathcal{L}\rho(t). \tag{3}$$

Here, the first term on the right-hand side of Eq. (3) describes the unitary evolution of the system, and the second term represents the decoherence of the system coupled to environments.

One can describe the influence of the detector by the following density-matrix elements [11],

$$\begin{aligned} \dot\rho_{ll} &= -i\Delta(\rho_{lr} - \rho_{rl}), \\ \dot\rho_{lr} &= i\varepsilon\rho_{lr} + i\Delta(\rho_{lr} - \rho_{rl}) - \frac{\Gamma_d}{2}\rho_{lr}, \end{aligned} \tag{4}$$

where $\rho_{rr} = 1 - \rho_{ll}$, $\rho_{rl} = \rho_{lr}^*$. The diagonal terms ρ_{ll} and ρ_{rr} are the probabilities of finding the electron in the left and right dots, respectively; whereas the off-diagonal terms generate an exponential damping with the decoherence rate $\Gamma_d = (\sqrt{D} - \sqrt{D'})^2$. Here, $D = 2\pi|\Omega_{12}|^2\rho_1\rho_2(\mu_1 - \mu_2)$, $D' = 2\pi|\Omega_{12}^{'}|^2\rho_1\rho_2(\mu_1 - \mu_2)$, and $\rho_{1,2}$ is the density of states in the reservoirs [45]. Finally, the decoherence process leads to a vanishing of the off-diagonal element in Eq. (4) in long-time limit $t \to \infty$.

Now, we relate the qubit dynamical behavior for the particle number reduced density matrix. The density-matrix elements of the system ρ_{ij} can be written as a sum of the components $\rho_{ij}^{(n)}$. The index n represents the number of electrons accumulated in the detector and recorded in a given time t. Then, the cumulant generating function can be constructed by [46]

$$\rho_{ij}(x,t) = \sum_{n=0}^{\infty} \rho_{ij}^{(n)}(t) e^{-nx}, \tag{5}$$

where x is a counting parameter. In order to study the quantum measurement, we exploit the nth component $\rho^{(n)}(t)$ of the reduced density matrix of the DQD system which satisfies the time evolution [33],

$$\dot\rho^{(n)}(t) = L\rho^{(n)}(t) + L_J\rho^{(n-1)}(t), \tag{6}$$

where L is the continuous evolution of the system and L_J describes the quantum jump of transferred electrons [33].

To address the dynamics of electrons clearly, we introduce the Bloch vectors [7,13],

$$\begin{aligned} \mathcal{X}(x,t) &= \rho_{lr} + \rho_{rl}, \\ \mathcal{Y}(x,t) &= \frac{1}{i}(\rho_{lr} - \rho_{rl}), \\ \mathcal{Z}(x,t) &= \rho_{ll} - \rho_{rr}, \end{aligned} \tag{7}$$

and in order to calculate the dynamical properties conveniently, we propose an additional vector,

$$N(x,t) = \rho_{ll} + \rho_{rr}, \tag{8}$$

to characterize the statistical fluctuations in the quantum measurement.

We utilize the additional vector to perform the derivative of $N(x,t)$ with respect to x. Once the Bloch vectors with the additional vector are obtained, we easily can derive the statistical properties related to the dynamical evolution of the system. Solving the additional vector, the cumulants of the electrons' counting can be written as

$$\langle N^{(k)}\rangle = (-1)^k \frac{\partial^k}{\partial x^k} N(x,t)\Big|_{x=0}. \tag{9}$$

Furthermore, the average current and Fano factor can be obtained at $x = 0$,

$$\begin{aligned} \dot I(t) &= -e\langle \dot N^{(1)}\rangle, \\ F(t) &= -\frac{\langle N^{(2)}\rangle - \langle N^{(1)}\rangle^2}{\langle N^{(1)}\rangle}. \end{aligned} \tag{10}$$

The probability that n electrons transferred in the time interval between 0 and t is obtained

$$P_n(t) = (-1)^n \frac{1}{n!}\frac{\partial^n}{\partial x^n} N(x,t)\Big|_{x\to\infty}, \tag{11}$$

and then the average waiting time is expressed as

$$\langle \tau \rangle = \int_0^\infty P_0(t)dt. \tag{12}$$

During the past several years, it has been an interesting topic to study the properties of the quantum dissipative dynamics in the qubit evolution. The discussions of measurement of the quantum dynamics in dissipative and pure dephasing environments are given in the next two sections, respectively.

III. THE DYNAMICAL PROPERTIES IN THE DISSIPATIVE ENVIRONMENT

In this section, we discuss the measurement of the dynamical process in the dissipative environment. We diagonalize the Hamiltonian H_S by considering the coupling with the environment. Then, the energy eigenstates are described by the bonding state and antibonding state [47],

$$a_L = \sin\frac{\theta}{2}a_l - \cos\frac{\theta}{2}a_r, \quad a_R = \cos\frac{\theta}{2}a_l + \sin\frac{\theta}{2}a_r, \tag{13}$$

where $\theta = \arctan(2\Delta/\varepsilon)$. The Hamiltonian of the DQD in Eq. (1) can be rewritten as $H_S = \frac{\bar{\varepsilon}}{2}(a_L^\dagger a_L - a_R^\dagger a_R)$ with $\bar{\varepsilon} = (\varepsilon^2 + 4\Delta^2)^{1/2}$. Thus the DQD system can be transformed into a parallel two-level system [48].

In the presence of the dissipative environment, the density matrix is given by [45]

$$\dot{\rho}_{\rm LL} = -\Gamma_r \rho_{\rm LL}, \quad \dot{\rho}_{\rm LR} = i\bar{\varepsilon}\rho_{\rm LR} - \frac{\Gamma_r}{2}\rho_{\rm LR}, \tag{14}$$

where Γ_r is the relaxation rate. The density-matrix element $\rho_{\rm LL}$ clearly manifests an exponential decay of the electron from the upper level to the ground level. Now we consider the qubit behavior in the presence of the interaction with the detector. The corresponding continuous evolution L reads

$$L = \begin{pmatrix} -\frac{\Gamma_r}{4}\left(1-\frac{\varepsilon}{\bar{\varepsilon}}\right)^2 - D & \frac{\Gamma_r}{4}\left(1+\frac{\varepsilon}{\bar{\varepsilon}}\right)^2 & i\Delta - \frac{\Gamma_r}{2}\frac{\Delta\varepsilon}{\bar{\varepsilon}^2} & -i\Delta - \frac{\Gamma_r}{2}\frac{\Delta\varepsilon}{\bar{\varepsilon}^2} \\ \frac{\Gamma_r}{4}\left(1-\frac{\varepsilon}{\bar{\varepsilon}}\right)^2 & -\frac{\Gamma_r}{4}\left(1+\frac{\varepsilon}{\bar{\varepsilon}}\right)^2 - D' & -i\Delta + \frac{\Gamma_r}{2}\frac{\Delta\varepsilon}{\bar{\varepsilon}^2} & i\Delta + \frac{\Gamma_r}{2}\frac{\Delta\varepsilon}{\bar{\varepsilon}^2} \\ i\Delta + \Gamma_r\frac{\Delta}{\bar{\varepsilon}}\left(1-\frac{\varepsilon}{2\bar{\varepsilon}}\right) & -i\Delta + \Gamma_r\frac{\Delta}{\bar{\varepsilon}}\left(1+\frac{\varepsilon}{2\bar{\varepsilon}}\right) & -i\varepsilon - \Gamma_r\frac{\Delta^2}{\bar{\varepsilon}^2} - \frac{\Gamma_r}{2} - \frac{D+D'}{2} & -\Gamma_r\frac{\Delta^2}{\bar{\varepsilon}^2} \\ -i\Delta + \Gamma_r\frac{\Delta}{\bar{\varepsilon}}\left(1-\frac{\varepsilon}{2\bar{\varepsilon}}\right) & i\Delta + \Gamma_r\frac{\Delta}{\bar{\varepsilon}}\left(1+\frac{\varepsilon}{2\bar{\varepsilon}}\right) & -\Gamma_r\frac{\Delta^2}{\bar{\varepsilon}^2} & i\varepsilon - \Gamma_r\frac{\Delta^2}{\bar{\varepsilon}^2} - \frac{\Gamma_r}{2} - \frac{D+D'}{2} \end{pmatrix}, \tag{15}$$

and the quantum jump L_J writes

$$L_J = \begin{pmatrix} D & 0 & 0 & 0 \\ 0 & D' & 0 & 0 \\ 0 & 0 & \sqrt{DD'} & 0 \\ 0 & 0 & 0 & \sqrt{DD'} \end{pmatrix}. \tag{16}$$

We deduce the derivation of the time evolution of the Bloch equations with respect to x by reducing Eqs. (15) and (16) according to Eqs. (7) and (8). Correspondingly, the current, the Fano factor, and the waiting time can be calculated accurately via the Bloch equations with the counting field x. The electron charge is set to be $e = 1$.

Now we demonstrate that the dynamical properties are rather distinct from the changing of the level displacement in Fig. 2. In addition, the influence of the decoherence induced by the detector and the environment is discussed. The average current shows a typical platform structure for long times as displayed in Fig. 2(a). The figure shows that the current sharply increases around $\varepsilon = 0$ and tends to be steady with the increase in ε when the probability of the transferred electron is accelerated rapidly and the transport channels are open. We find that the different relaxation rates Γ_r slightly affect the stationary current in Fig. 2(a). The results are qualitatively consistent with those in Ref. [11]. Figure 2(c) shows that the current is sensitive to decoherence rates. The platform goes up as the decoherence rates go from $\Gamma_d = 0.1\Delta$ to $\Gamma_d = 0.3\Delta$. This is mainly because the quantum coherence between electrons strongly influences the values of the current.

The Fano factor is shown in Figs. 2(b) and 2(d), respectively, as a function of the level displacement ε for different relaxation and decoherence rates. On the whole the two figures both display asymmetrical structures due to the relaxation process. In addition, the Fano factor exhibits a crossover from weak sub-Poissonian statistics with a dip around $\varepsilon = 0$ to super-Poissonian statistics and tends to be Poissonian for large level displacement. We emphasize that the apparent super-Poissonian statistics implies that the behavior of electron transfer is similar to the dynamical channel blockade [21,30,49,50]. As shown in Fig. 2(b), the reduction of the Fano factor peaks is particularly notable as the growth of relaxation rates, which generally manifests the noise suppression owing to the coupling with the dissipative environment. Inversely, in Fig. 2(d) the values of the Fano factor become large with the increase in decoherence rates for a given ε (see the red, blue, and green curves), restricting the transferred electrons which can be supposed to be partially coherent and lead to disordered electron tunneling.

Furthermore, the value of the Fano factor $F = 1$ forms a classical Poisson process with the increase in level displacement ε, which demonstrates there is no correlation

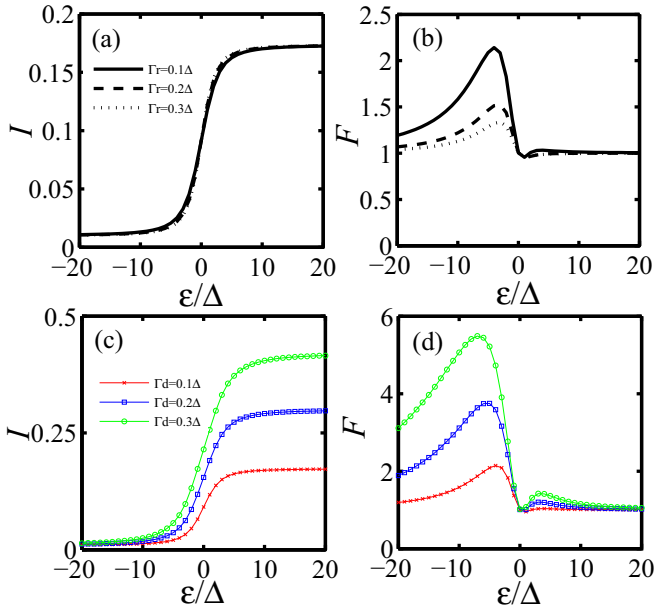

FIG. 2. The current and Fano factor versus the level displacement ε in the dissipative environment. (a) The current and (b) the Fano factor for different relaxation rates: $\Gamma_r = 0.1\Delta$ (the black solid curve), $\Gamma_r = 0.2\Delta$ (the black dashed curve), and $\Gamma_r = 0.3\Delta$ (the black dotted curve). (c) The current and (d) the Fano factor for different decoherence rates: $\Gamma_d = 0.1\Delta$ (the red curve), $\Gamma_d = 0.2\Delta$ (the blue curve), and $\Gamma_d = 0.3\Delta$ (the green curve).

between successive electron tunneling [36,49]. The Fano factor surprisingly shows weak sub-Poissonian behavior in both Figs. 2(b) and 2(d) at $\varepsilon = 0$. This indicates that the sequential tunneling [51] happened in this regime, which strongly suppresses the Fano factor and causes the dip. We can conclude that the current and Fano factor are more sensitive to the decoherence rates than the relaxation rates. Specifically, one can accurately measure the decoherence or relaxation rates of the qubit via the Fano factor.

A complementary view on dynamical properties is provided by the distribution of waiting time which fully captures a random walk in time [23]. In Fig. 3, the average waiting time increases rapidly with the decrease in ε for $\varepsilon < 0$, whereas the values increase slowly with the growth of ε for $\varepsilon > 0$. The obvious dip which signifies shorter waiting times in Fig. 3 corresponds to the substantial changes in current around $\varepsilon = 0$ in Figs. 2(a) and 2(c). Figure 3(a) shows that different relaxation rates do not affect the average waiting time (three curves coincide) for $\varepsilon < 0$, whereas the values (see the solid, the long dashed, and the short dashed curves) smoothly ascend with the increase in the relaxation rates for $\varepsilon > 0$. Overall, the results exhibit the changing tendency of the average waiting time is consistent with the current in Fig. 2. We find that the appearance of the flat and largest values of the average waiting time is mainly due to the electron localization in the DQD, which results in the super-Poissonian statistics in Figs. 2(b) and 2(d). Moreover, the steady values decline in Fig. 3(b) with the increase in decoherence rates from 0.1Δ to 0.3Δ (see the red, blue, and green curves).

IV. THE DYNAMICAL PROPERTIES IN THE PURE DEPHASING ENVIRONMENT

In this section, we study the dynamical properties of measurement in the pure dephasing environment without energy relaxation. In this case the evolution of the density matrix is given by

$$\dot{\rho}_{\mathrm{LL}} = 0, \quad \dot{\rho}_{\mathrm{LR}} = i\bar{\varepsilon}\rho_{\mathrm{LR}} - \Gamma_\phi \rho_{\mathrm{LR}}, \tag{17}$$

where Γ_ϕ is the dephasing rate. Note that the off-diagonal density-matrix element ρ_{LR} vanishes in the limit $t \to \infty$. We employ the same bonding state and antibonding state in Eq. (13). Using the Bloch equations with the additional vector that we mentioned in Sec. II, the corresponding continuous evolution L is given by

$$L = \begin{pmatrix} -2\Gamma_\phi \frac{\Delta^2}{\bar{\varepsilon}^2} - D & 2\Gamma_\phi \frac{\Delta^2}{\bar{\varepsilon}^2} & i\Delta + \Gamma_\phi \frac{\Delta\varepsilon}{\bar{\varepsilon}^2} & -i\Delta + \Gamma_\phi \frac{\Delta\varepsilon}{\bar{\varepsilon}^2} \\ 2\Gamma_\phi \frac{\Delta^2}{\bar{\varepsilon}^2} & -2\Gamma_\phi \frac{\Delta^2}{\bar{\varepsilon}^2} - D' & -i\Delta - \Gamma_\phi \frac{\Delta\varepsilon}{\bar{\varepsilon}^2} & i\Delta - \Gamma_\phi \frac{\Delta\varepsilon}{\bar{\varepsilon}^2} \\ i\Delta + \Gamma_\phi \frac{\Delta\varepsilon}{\bar{\varepsilon}^2} & -i\Delta - \Gamma_\phi \frac{\Delta\varepsilon}{\bar{\varepsilon}^2} & -i\varepsilon - \frac{\Gamma_\phi}{2}\left(1 + \frac{\varepsilon^2}{\bar{\varepsilon}^2}\right) - \frac{D+D'}{2} & 2\Gamma_\phi \frac{\Delta^2}{\bar{\varepsilon}^2} \\ -i\Delta + \Gamma_\phi \frac{\Delta\varepsilon}{\bar{\varepsilon}^2} & i\Delta - \Gamma_\phi \frac{\Delta\varepsilon}{\bar{\varepsilon}^2} & 2\Gamma_\phi \frac{\Delta^2}{\bar{\varepsilon}^2} & i\varepsilon - \frac{\Gamma_\phi}{2}\left(1 + \frac{\varepsilon^2}{\bar{\varepsilon}^2}\right) - \frac{D+D'}{2} \end{pmatrix}, \tag{18}$$

and the quantum jump L_J is the same as expressed in Eq. (16).

The current and Fano factor versus the level displacement are plotted in Fig. 4 for different dephasing and decoherence rates, respectively, by Eqs. (16) and (18). The figures show that both the current and the Fano factor are symmetrical around $\varepsilon = 0$. We find that the current and the Fano factor are not sensitive at all for different dephasing rates (three curves coincide) in Figs. 4(a) and 4(b). The Fano factor reaches a local minimum at $\varepsilon = 0$, grows with increasing ε, but decreases rapidly with large displacement for $F = 1$. Noticeably, the figure shows clearly that a double peak in the Fano factor refers to a coherent tunneling regime. It is found that a dynamical channel blockade mechanism is developed, which leads to a profound super-Poissonian noise.

It is worth noting that the current reaches a maximum around $\varepsilon = 0$ and tends to a smooth platform for small ε in Fig. 4(a), which is attributed to the subtle change in current in the pure dephasing process. Figure 4(c) displays that the area of the platform extends with the increase in decoherence rates. This shows that the coupling to the detector would enhance electron localization in one dot. Consequently, electron transfer would be suppressed, and the dwelling time of an electron increased, which leads to the quantum Zeno effect. Compared with Figs. 4(b) and 4(d), because of this effect, the

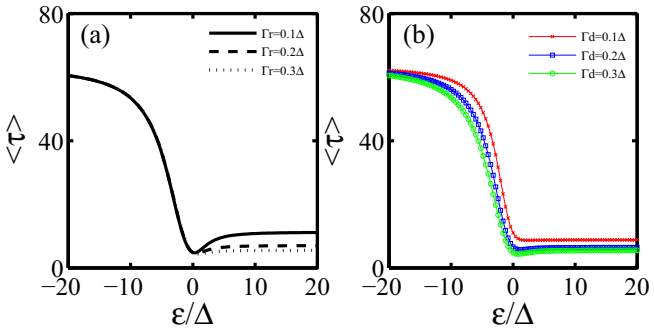

FIG. 3. The average waiting time $\langle\tau\rangle$ calculated from the Bloch equations for (a) different relaxation rates: $\Gamma_r = 0.1\Delta$ (the black solid curve), $\Gamma_r = 0.2\Delta$ (the black dashed curve), and $\Gamma_r = 0.3\Delta$ (the black dotted curve) and (b) different decoherence rates: $\Gamma_d = 0.1\Delta$ (the red curve), $\Gamma_d = 0.2\Delta$ (the blue curve), and $\Gamma_d = 0.3\Delta$ (the green curve).

Fano factor is magnified and broadened as the decoherence rates increase from $\Gamma_d = 0.1\Delta$ to $\Gamma_d = 0.3\Delta$.

As discussed above and comparing Figs. 2(b) and 4(b), we can conclude that the noise suppression is sensitive to the energy relaxation of the system whereas the dephasing of the system hardly changes the noise fluctuations. This is consistent completely with the conclusion made in Ref. [39]. There exists a quantum Zeno effect which freezes the evolution of a quantum system associated with the suppression of electron transfer subject to QPC measurement [43,52–54] and the measurement can manipulate the system dynamics by changing the strength of the interaction with the detector [42,55].

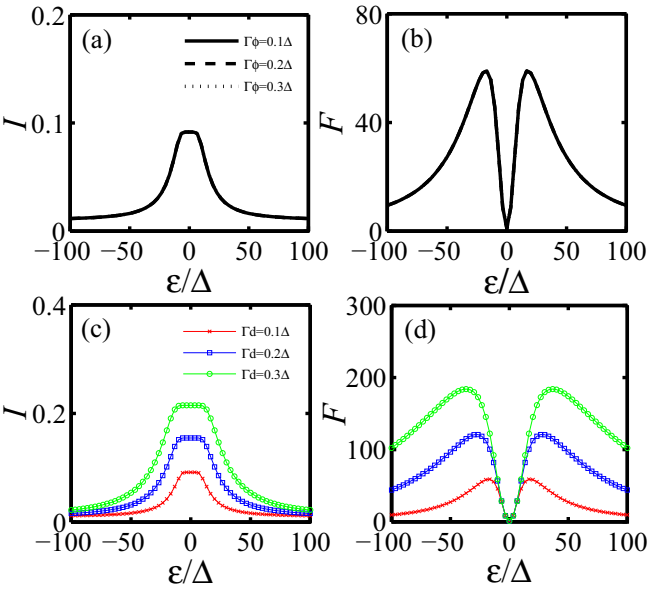

FIG. 4. The current and Fano factor versus the level displacement ε in the pure dephasing environment. (a) The current and (b) the Fano factor for different dephasing rates: $\Gamma_\phi = 0.1\Delta$ (the black solid curve), $\Gamma_\phi = 0.2\Delta$ (the black dashed curve), and $\Gamma_\phi = 0.3\Delta$ (the black dotted curve). (c) The current and (d) the Fano factor for different decoherence rates: $\Gamma_d = 0.1\Delta$ (the red curve), $\Gamma_d = 0.2\Delta$ (the blue curve), and $\Gamma_d = 0.3\Delta$ (the green curve).

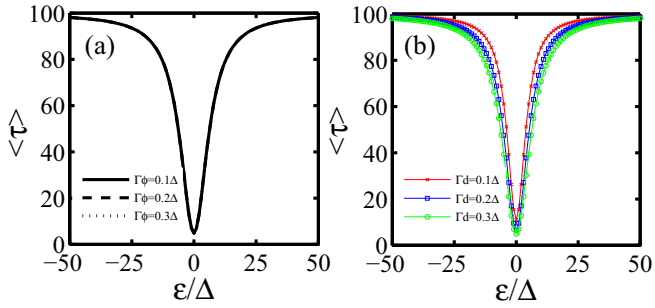

FIG. 5. The average waiting time $\langle\tau\rangle$ calculated from the Bloch equations for (a) different dephasing rates: $\Gamma_\phi = 0.1\Delta$ (the black solid curve), $\Gamma_\phi = 0.2\Delta$ (the black dashed curve), and $\Gamma_\phi = 0.3\Delta$ (the black dotted curve) and (b) different decoherence rates: $\Gamma_d = 0.1\Delta$ (the red curve), $\Gamma_d = 0.2\Delta$ (the blue curve), and $\Gamma_d = 0.3\Delta$ (the green curve).

The symmetrical structures of the average waiting time distribution do not change as the dephasing rates increase from 0.1Δ to 0.3Δ but exhibit the steady decline of values as the decoherence rates increase from 0.1Δ to 0.3Δ in Fig. 5. In addition, the largest of the steady values reveals the reason for the super-Poissonian statistics. The coupling with environment would enhance electron localization in one DQD. Furthermore, for the same reason the dip in Fig. 5 corresponds to the peak of current in Figs. 4(a) and 4(c). The good agreement between the distribution of the average waiting time and the current is presented.

V. CONCLUSIONS

In conclusion, we study quantum measurement of a DQD by Bloch equations with an additional vector and concentrate on the intriguing properties arising from the internal dynamics induced by two different kinds of environments. It is shown that, in the dissipative environment, the Fano factor exhibits clear enhancement associated with decoherence rates and suppression related to relaxation rates whereas the current is not sensitive to different relaxation rates. We show that the relaxation process results in the asymmetry of the Fano factor and the patterns obviously are changed by the decoherence rates. The dynamical channel blockade effect takes place in the presence of the level displacement and which leads to the super-Poissonian noise. In the pure dephasing environment, both the current and the Fano factor are symmetrical. We emphasize that the quantum Zeno effect has been formed which effectively localizes the electron in one of the DQD leading to the enhancement of the Fano factor. Moreover, the results illustrate that the distribution of the average waiting time exhibits good agreement with the variation tendency of the current. We predict that both the relaxation and the decoherence rates can be measured through the Fano factor. The advantages of our method possess useful ways in comparison with the previous methods, so our paper provides an effective tool to analyze dynamical properties. More physical quantities of mesoscopic transport can be studied continuously via our method, such as the skewness, kurtosis, and so on. Our results and analysis can be used properly to explore new effects of mesoscopic systems.

ACKNOWLEDGMENT

This work was supported by the Natural Science Foundation of Shandong Province Grant No. ZR2014AM030.

[1] A. E. Petrova and S. M. Stishov, Phys. Rev. B **86**, 174407 (2012).
[2] X. Zhu, Y. Zhang, S. Pang, C. Qiao, Q. Liu, and S. Wu, Phys. Rev. A **84**, 052111 (2011).
[3] N. Brunner and C. Simon, Phys. Rev. Lett. **105**, 010405 (2010).
[4] T. Baumgratz, M. Cramer, and M. B. Plenio, Phys. Rev. Lett. **113**, 140401 (2014).
[5] E. Bagan, J. A. Bergou, S. S. Cottrell, and M. Hillery, Phys. Rev. Lett. **116**, 160406 (2016).
[6] D. Mozyrsky, L. Fedichkin, S. A. Gurvitz, and G. P. Berman, Phys. Rev. B **66**, 161313 (2002).
[7] A. Chantasri and A. N. Jordan, Phys. Rev. A **92**, 032125 (2015).
[8] N. Katz, M. Neeley, M. Ansmann, R. C. Bialczak, M. Hofheinz, E. Lucero, A. O'Connell, H. Wang, A. N. Cleland, J. M. Martinis, and A. N. Korotkov, Phys. Rev. Lett. **101**, 200401 (2008).
[9] G. P. Zhao, Y. H. Zhang, X. J. Cai, X. L. Xu, and L. S. Kang, Physica E **84**, 10 (2016).
[10] P. J. Liebermann and F. K. Wilhelm, Phys. Rev. Appl. **6**, 024022 (2016).
[11] S. A. Gurvitz, L. Fedichkin, D. Mozyrsky, and G. P. Berman, Phys. Rev. Lett. **91**, 066801 (2003).
[12] S. A. Gurvitz and D. Mozyrsky, Phys. Rev. B **77**, 075325 (2008).
[13] H. Wiseman and G. Milburn, *Quantum Measurement and Control* (Cambridge University Press, Cambridge, UK, 2009).
[14] U. Hartmann and F. K. Wilhelm, Phys. Rev. B **75**, 165308 (2007).
[15] T. Hayashi, T. Fujisawa, H. D. Cheong, Y. H. Jeong, and Y. Hirayama, Phys. Rev. Lett. **91**, 226804 (2003).
[16] R. Aguado and T. Brandes, Phys. Rev. Lett. **92**, 206601 (2004).
[17] R. Sánchez, S. Kohler, P. Hänggi, and G. Platero, Phys. Rev. B **77**, 035409 (2008).
[18] S.-H. Ouyang, C.-H. Lam, and J. Q. You, Phys. Rev. B **81**, 075301 (2010).
[19] R. Sánchez, G. Platero, and T. Brandes, Phys. Rev. Lett. **98**, 146805 (2007).
[20] Y. M. Blanter and M. Büttiker, Phys. Rep. **336**, 1 (2000).
[21] G. Kießlich, E. Schöll, T. Brandes, F. Hohls, and R. J. Haug, Phys. Rev. Lett. **99**, 206602 (2007).
[22] G. Kießlich, A. Wacker, and E. Schöll, Phys. Rev. B **68**, 125320 (2003).
[23] M. Albert, G. Haack, C. Flindt, and M. Büttiker, Phys. Rev. Lett. **108**, 186806 (2012).
[24] M. Esposito, U. Harbola, and S. Mukamel, Rev. Mod. Phys. **81**, 1665 (2009).
[25] A. A. Clerk, M. H. Devoret, S. M. Girvin, F. Marquardt, and R. J. Schoelkopf, Rev. Mod. Phys. **82**, 1155 (2010).
[26] A. N. Korotkov and D. V. Averin, Phys. Rev. B **64**, 165310 (2001).
[27] A. N. Korotkov, Phys. Rev. B **63**, 085312 (2001).
[28] X.-Q. Li, P. Cui, and Y. J. Yan, Phys. Rev. Lett. **94**, 066803 (2005).
[29] H.-S. Goan, G. J. Milburn, H. M. Wiseman, and H. B. Sun, Phys. Rev. B **63**, 125326 (2001).
[30] W. Belzig, Phys. Rev. B **71**, 161301 (2005).
[31] D. V. Averin and E. V. Sukhorukov, Phys. Rev. Lett. **95**, 126803 (2005).
[32] Y. Okazaki, S. Sasaki, and K. Muraki, Phys. Rev. B **87**, 041302 (2013).
[33] C. Emary, D. Marcos, R. Aguado, and T. Brandes, Phys. Rev. B **76**, 161404 (2007).
[34] C. W. Groth, B. Michaelis, and C. W. J. Beenakker, Phys. Rev. B **74**, 125315 (2006).
[35] R. López, R. Aguado, and G. Platero, Phys. Rev. B **69**, 235305 (2004).
[36] C. Flindt, T. Novotný, and A.-P. Jauho, Phys. Rev. B **70**, 205334 (2004).
[37] S. Gustavsson, R. Leturcq, T. Ihn, K. Ensslin, M. Reinwald, and W. Wegscheider, Phys. Rev. B **75**, 075314 (2007).
[38] S. Gustavsson, R. Leturcq, B. Simovič, R. Schleser, P. Studerus, T. Ihn, K. Ensslin, D. C. Driscoll, and A. C. Gossard, Phys. Rev. B **74**, 195305 (2006).
[39] A. Shimizu and M. Ueda, Phys. Rev. Lett. **69**, 1403 (1992).
[40] W. M. Itano, D. J. Heinzen, J. J. Bollinger, and D. J. Wineland, Phys. Rev. A **41**, 2295 (1990).
[41] S. Pascazio and M. Namiki, Phys. Rev. A **50**, 4582 (1994).
[42] J. Ruseckas and B. Kaulakys, Phys. Rev. A **63**, 062103 (2001).
[43] K. Koshino and A. Shimizu, Phys. Rep. **412**, 191 (2005).
[44] S. A. Gurvitz, Phys. Rev. B **56**, 15215 (1997).
[45] S. A. Gurvitz and Y. S. Prager, Phys. Rev. B **53**, 15932 (1996).
[46] A. A. Budini, Phys. Rev. E **82**, 061106 (2010).
[47] J. Luo, H. Jiao, Y. Shen, G. Cen, X.-L. He, and C. Wang, J. Phys.: Condens. Matter **23**, 145301 (2013).
[48] C. Xu and M. G. Vavilov, Phys. Rev. B **88**, 195307 (2013).
[49] F. Bodoky, W. Belzig, and C. Bruder, Phys. Rev. B **77**, 035302 (2008).
[50] A. Carmi and Y. Oreg, Phys. Rev. B **85**, 045325 (2012).
[51] G. Kießlich, P. Samuelsson, A. Wacker, and E. Schöll, Phys. Rev. B **73**, 033312 (2006).
[52] K. Koshino and A. Shimizu, Phys. Rev. Lett. **92**, 030401 (2004).
[53] D. Suter and G. A. Álvarez, Rev. Mod. Phys. **88**, 041001 (2016).
[54] T. P. Altenmüller and A. Schenzle, Phys. Rev. A **49**, 2016 (1994).
[55] A. H. Kiilerich and K. Mølmer, Phys. Rev. A **92**, 032124 (2015).